Electrochimica Acta 56 (2011) 1213–1218

Contents lists available at ScienceDirect

Electrochimica Acta

journal homepage: www.elsevier.com/locate/electacta

Electrochemical characteristics and intercalation mechanism of ZnS/C composite as anode active material for lithium-ion batteries

Li He[a], Xiao-Zhen Liao[a,*], Ke Yang[a], Yu-Shi He[a], Wen Wen[b], Zi-Feng Ma[a,**]

[a] Institute of Electrochemical and Energy Technology, Department of Chemical Engineering, Shanghai Jiao Tong University, Shanghai 200240, China
[b] Shanghai Synchrotron Radiation Facility, Shanghai Institute of Applied Physics, Chinese Academy of Sciences, Shanghai 201204, China

ARTICLE INFO

Article history:
Received 6 September 2010
Received in revised form 1 November 2010
Accepted 7 November 2010
Available online 13 November 2010

Keywords:
ZnS/C composite
Anode active materials
Rate capability
Lithium ion batteries
Intercalation mechanism

ABSTRACT

ZnS/C composites were synthesized by a combined precipitation with carbon coating method. Morphology and structure of the as-prepared ZnS/C composite materials with carbon content of 4.6 wt%, 9.3 wt% and 11.4 wt% were characterized using TEM and XRD technique. TEM observation demonstrated that the ZnS/C (9.3 wt% C) composite showed excellent microstructure with 20–30 nm ZnS nanoparticles uniformly dispersed in conductive carbon network. Electrochemical tests showed that the ZnS/C (9.3 wt% C) composite presented superior performance with initial charge and discharge capacity of 1021.1 and 481.6 mAh/g at a high specific current of 400 mA/g, after 300 cycles, the discharge capacity of ZnS/C electrode still maintained at 304.4 mAh/g, with 63.2% of its initial capacity. The rate capability and low temperature performance of the ZnS/C (9.3 wt% C) composite were compared with commercial MCMB anode. The results showed that the ZnS/C (9.3 wt%) composite exhibited much better cycle capability and low temperature performance than MCMB anode. ZnS/C composite seems to be a promising anode active material for lithium ion batteries. Intercalation mechanism of the ZnS/C composites for lithium ion insertion–extraction is proposed based on the ex situ X-ray diffraction analysis incorporating with its electrochemical characteristics.

1. Introduction

The overall electrochemical performance of lithium ion batteries is mainly determined by the intrinsic properties of the electrode active materials. Advanced electrode active materials are required for the development of high performance lithium ion batteries with large reversible capacity, high rate capability and the ability to work at wide temperature range. Finding new cathode or anode active materials to improve the energy density are one of the most important goals for next-generation lithium ion batteries. Since graphite was introduced as anode active material for commercial lithium ion batteries application in 1990, many research works have focused on metallic alloy anode active materials, which might have higher energy density compared with commercial graphite anode active material. Because the higher theoretical specific capacity than those of carbon, Si-based anode materials are investigated worldwide since the pioneer work by Besenhard et al. [1], but the capacity degradation caused by volume distention are still not overcomed. Besides high capacity Si-based materials, other alloy or composites were also commonly investigated as anode active materials, such as Sn, Co, Ni, Fe, and SnNi alloy compounds [2,3].

Recently, zinc-based materials such as ZnO [4], Zn_3N_2 [5], Zn_3P_2 [6], Zn–Sn alloys [7,8], Si–Zn–C [9], ZnNiIn [10], $ZnCo_2O_4$ [11] are used as intercalation material for lithium ion batteries application. Fujieda et al. [12] and Wang et al. [13] discovered lithium–zinc alloy could be formed electrochemically, five phases of $LiZn_4$, Li_2Zn_5, $LiZn_2$, Li_2Zn_3 and LiZn existed in lithium–zinc alloy. On the other hand, some of sulphide was found as intercalation material. Tu and coworkers [14] prepared the SnS nanoparticles and applied as anode material, they found tin sulphide provides better cycle stability because the formation of Li_2S could perform as a buffer matrix for metal active phase. ZnS is an important inorganic semiconducting material used widely in displays, sensors, solar cells and lasers. Mohan Rao and coworkers [15] synthesized nanocrystalline ZnS by using hydrothermal method and demonstrated ZnS can be used as promising electrodes in electrochemical capacitor application. Wang et al. found that ZnS also exibited lithium insertion–disertion capability, and the capacity and stability of the reported ZnS material was still lower than other metallic alloy materials [16], but the raw material for synthesizing ZnS is cheaper than that of the well investigated SnS [17,18], so we think ZnS composites may become a promising anode active material if their electrochemical performance and stability improved. Carbon coat-

* Corresponding author. Tel.: +86 21 54744533.
** Corresponding author. Tel.: +86 21 54742894; fax: +86 21 54747717.
E-mail addresses: liaoxz@sjtu.edu.cn (X.-Z. Liao), zfma@sjtu.edu.cn (Z.-F. Ma).

0013-4686/$ – see front matter © 2010 Elsevier Ltd. All rights reserved.
doi:10.1016/j.electacta.2010.11.014

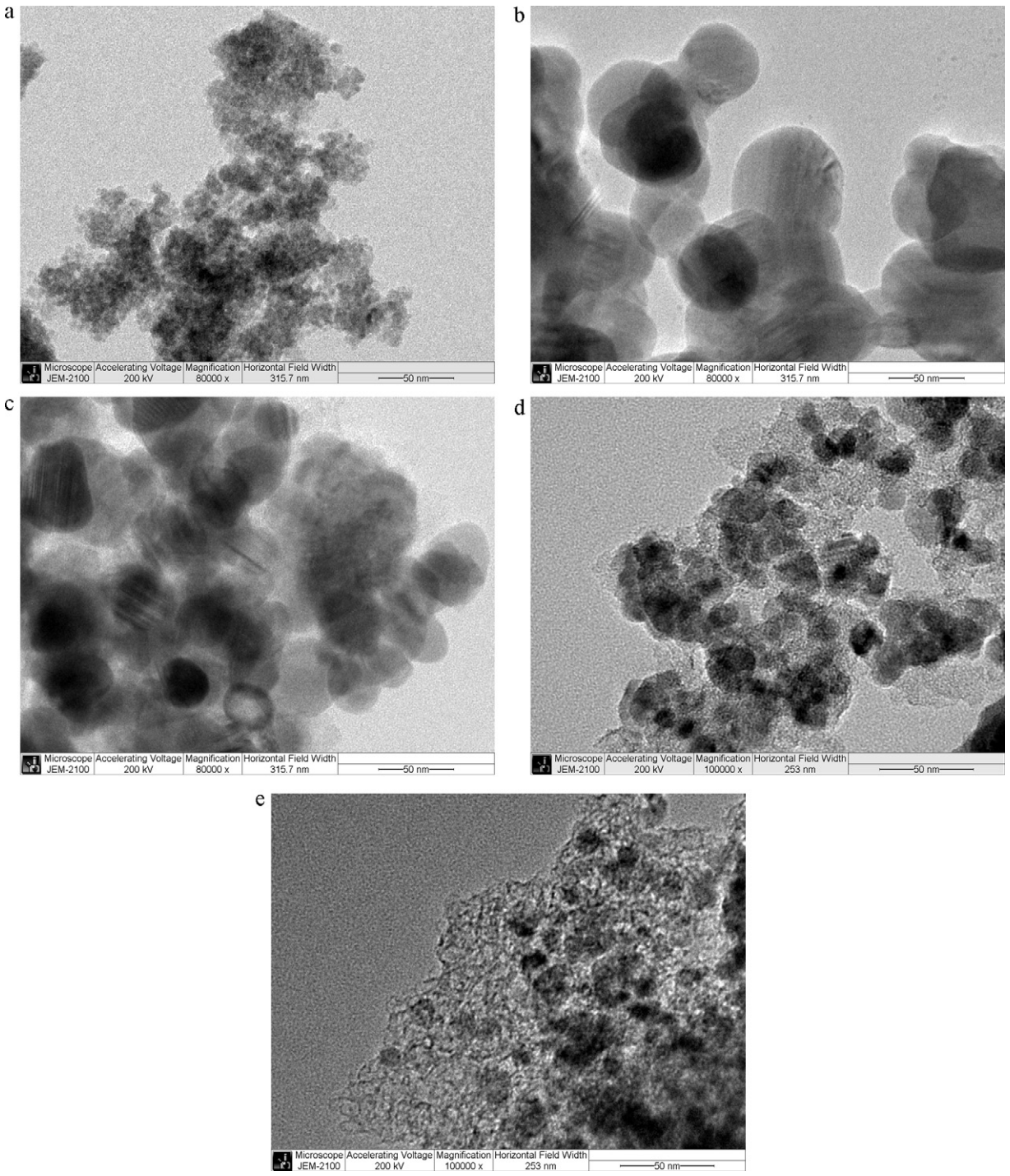

Fig. 1. TEM images of ZnS and ZnS/C composites: (a) dried ZnS precipitate, (b) bare ZnS, (c) ZnS/C (4.6 wt% C), (d) ZnS/C (9.3 wt% C) and (e) ZnS/C (11.4 wt% C).

ing has been commonly applied to improve the conductivity and electrochemical performance of electrode materials in lithium ion batteries. Up to now, we have found no literatures reporting on ZnS/C composite anode material for lithium ion batteries application. Herein, we firstly prepared ZnS/C composites by carbon coating and investigated its rate capabilities and temperature performance as anode active material for lithium ion batteries. The lithium insertion–extraction mechanism of the ZnS/C composite anode material is also investigated by ex situ X-ray diffraction analysis.

2. Experimental

ZnS nanoparticles were prepared by a precipitation method using $Na_2S{\cdot}9H_2O$ and $ZnCl_2{\cdot}4H_2O$ as reagents. In a typical procedure, the hydrate solution of zinc chloride was added in the sodium sulphide hydrate solution drop by drop with slow stirring at room temperature, and then stirred continuously at 60 °C for 2 h to form white precipitate. The resulting white precipitate was cooled down and filtered and washed with de-ionized water, and dried at 80 °C to obtain the dried ZnS precipitate. The dried ZnS precipitate mixed

with citric acid (CA) uniformly and then calcinated under argon at 700 °C for 90 min to obtain the ZnS/C composites. The weight ratio of CA to ZnS of 1:1, 2:1 and 3:1 were selected to prepare ZnS/C composites with different carbon contents. The carbon content of the ZnS/C composites was analyzed by a CHNS/O analyzer (PE 2400 II, Perkin Elmer, America). Corresponding to the weight ratio of CA to ZnS, the carbon content of the as-prepared ZnS/C composites attained to 4.60 wt%, 9.30 wt% and 11.4 wt%, respectively. The dried ZnS precipitate was also heat treated under argon at 700 °C for 90 min to obtain bare ZnS material for comparison. The morphology and structure of the as-prepared bare ZnS and ZnS/C composites were observed by X-ray diffraction (Cu Kα, Rigaku, Japan) and transmission electron microscopy (JEM-2100, JEOL Ltd., Japan).

Electrochemical performance of the prepared ZnS/C composites was measured using a 2025 coin cell assembled under argon atmosphere. The working electrodes were prepared using 75% ZnS/C powder, 15% acetylene black and 10% polyvinylidene fluoride. The mixture was coated on a copper foil and punched to electrode disks of ϕ14 mm. The ZnS/C working electrode was incorporated into cells with a lithium foil counter electrode, a Celgard 2400 separator and a 1.0 M $LiPF_6$/EC + DMC + DEC + EMC (1:1:1:3, v/v) electrolyte. Charge–discharge performance of the ZnS/C| Li cells was evaluated using a battery test system (LAND CT2001A model, Wuhan Jinnuo Electronics Co., Ltd.) in the voltage range of 0.02–2 V vs. Li/Li^+ at constant specific currents. The electrochemical capacity of the composites was evaluated on the active materials. Cyclic voltammetry was performed on the ZnS/C|| Li coin cell using a Solartron SI 1287 electrochemical interface controlled by Corr-ware. The voltage window is 0.02–2 V and the scan rate is 0.1 mV/s.

3. Results and discussion

The morphologies of the dried ZnS precipitate, bare ZnS and ZnS/C composites are shown in Fig. 1. It can be seen, the dried ZnS precipitate shows fine particles smaller than 5 nm (Fig. 1a). After heat treatment, particle size of bare ZnS obviously increased up to 50–80 nm (Fig. 1b). The as-prepared ZnS/C composites (Fig. 1c–e) exhibited minimized ZnS particle size compared with the bare ZnS due to the addition of citric acid in the precursor mixture as carbon source. It was obvious that particle agglomeration was alleviated as the carbon content increased. The ZnS/C (9.3 wt% C) composite shows appreciable morphology with fine ZnS particles (10–25 nm) uniformly dispersed in conductive carbon network. Fig. 2 presents the XRD patterns of the as prepared ZnS and ZnS/C composites. The dried ZnS precipitate showed the peaks of orthorhombic single ZnS phase (JCPDS file 77-2100). After heat treatment at 700 °C the ZnS particles were changed to a crystalline hexagonal phase with space group *P*63*mc* (JCPDS file 75-1547).

Cycling performance of the bare ZnS and ZnS/C composites with different carbon content was measured at a constant specific current of 400 mA/g, and illustrated in Fig. 3. It indicated that all of ZnS/C composites displays much better cycle performance than that of bare ZnS and carbon coating are beneficial to improve the electrochemical performance of ZnS anode material. The cycling performance improvement of the ZnS/C composites attribute to well dispersion of ZnS particle on carbon network and the ZnS particle size change. As can be seen from Fig. 1, when carbon content increased, the particle size of ZnS is remarkably minimized, which greatly enhanced the lithiumate/delithium process of the electrode. The ZnS/C (9.3 wt% C) composite exhibited the best cycling behavior with a stable specific capacity of 360.4 mAh/g after 100 cycles, due to the uniform dispersion of fine ZnS particles in conductive carbon network (Fig. 1d). When the carbon content increased to 11.4 wt%, the relative content of ZnS decreased and the total capacity of the composite was reduced as well. Hereafter, the ZnS/C (9.3 wt% C) composite was selected as anode active material to investigate the electrochemical behavior and the lithium insertion–extraction mechanism of ZnS/C electrode. Hereby, for simplification, ZnS/C electrode will indicates ZnS/C (9.3 wt% C) composite in following discussion.

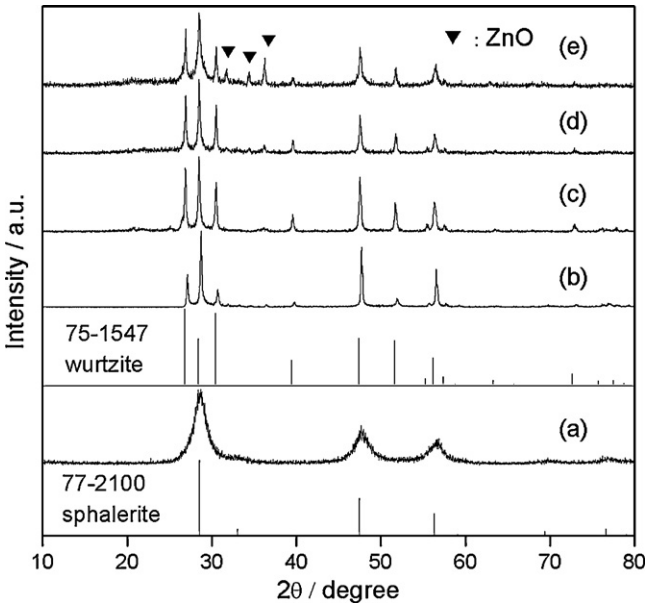

Fig. 2. XRD patterns of ZnS and ZnS/C composites: (a) dried ZnS precipitate, (b) bare ZnS, (c) ZnS/C (4.6 wt% C), (d) ZnS/C (9.3 wt% C) and (e) ZnS/C (11.4 wt% C).

Fig. 4 shows the typical galvanostatic cycling profiles of the ZnS/C electrode at a specific current of 400 mA/g. In the first charge process (lithium insertion), the potential dropped rapidly to 0.9 V and exhibited a charge plateau between 0.9 and 0.63 V, which might correspond to the decomposition of ZnS into Zn and the formation of Li_2S. At the following reaction stage, the potential drops slowly from 0.6 V to 0.02 V, and probably corresponding to the Li_xZn alloy formation. The charge capacity attained at 1021.1 mAh/g in the first cycle, while the discharge capacity was only 481.6 mAh/g. In the second and subsequent cycles, the difference between charge and discharge capacity gradually decreased, and after 10 cycles they are almost the same, more longer cycling performance of the ZnS/C electrode was illustrated in inset within Fig. 4. After 300

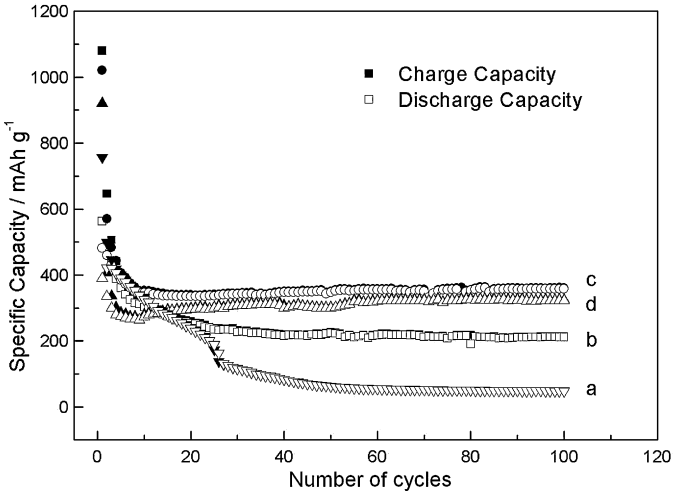

Fig. 3. Cycling performance of the various ZnS/C composites with different carbon contents at the specific current of 400 mA/g. (a) bare ZnS, (b) ZnS/C (4.6 wt% C), (c) ZnS/C (9.3 wt% C) and (d) ZnS/C (11.4 wt% C).

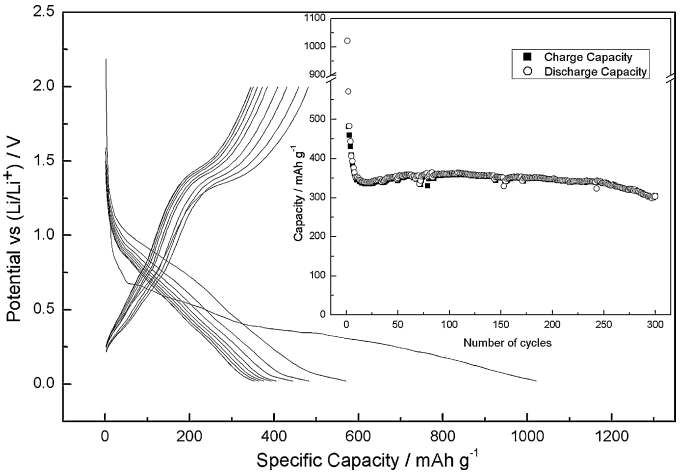

Fig. 4. Charge and discharge profiles and the cycling performance of ZnS/C (9.3 wt% C) electrode at the specific current of 400 mA/g.

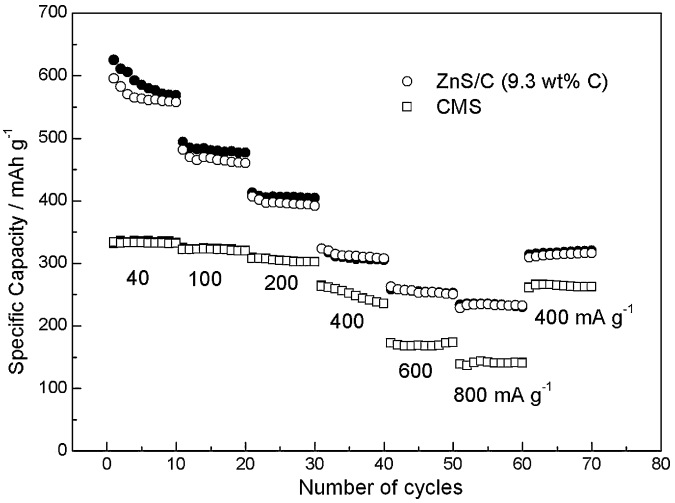

Fig. 6. Comparison of rate capability of the ZnS/C (9.3 wt% C) anode and commercial MCMB anode with a charge–discharge specific current range from 40, 100, 200, 400, 600 to 800 mA/g.

cycles, the discharge capacity of ZnS/C electrode still maintained at 304.4 mAh/g, which 63.2% of its initial capacity. This good cycling performance of the ZnS/C electrode may be attributed to the good conductive carbon matrix and also the resulting Li_2S, which may hinder the volume expansion of the active electrode.

Cyclic voltammetry measurements for the ZnS/C electrode were conducted at a scanning rate of 0.1 mV/s over potential range from 2.0 to 0.02 V. The CV curves are shown in Fig. 5. It can be seen, in the first scanning cycle, two broad reduction peaks appeared in the potential range of 1.0–0.6 V and 0.6–0.05 V, respectively. The first reduction peak range from 1.0 to 0.6 V is ascribed to the decomposition of ZnS into Zn and the formation of Li_2S. The second reduction peak in the potential range of 0.6–0.05 V can be attributed to the subsequent reaction of lithium ions with Zn metal. Solid electrolyte interface (SEI) film might also form on the surface of electrode during the first cathodic scanning process, which caused part of the irreversible capacity. During the anodic scanning process, four anodic peaks are observed in the potential range of 0.2–0.6 V indicating that Li was delithiated by several steps. Correspondingly, a series of cathodic peaks corresponding to lithium intercalation in zinc metal appeared in the potential range of 0.6–0.05 V in the subsequence scanning cycles.

These results indicate that the lithium–zinc alloy shows several phases with lithium content increases [12,13,19]. Another anodic peak at 1.3 V is attributed to the regeneration of ZnS.

Fig. 6 shows the rate performance of ZnS/C anode at different specific currents of 200, 400, 600 and 800 mAh/g. For comparison, the rate performance of the commercial MCMB anode was also tested in the same condition. It can be seen that the discharge capacity of ZnS/C decreased with the specific current increasing from 406 mAh/g (at 200 mA/g) to 323.3, 262.5 and 235.2 mAh/g at 400, 600 and 800 mA/g, respectively. However, under all specific currents, the capacities of ZnS/C anode are greater than that of MCMB anode. The ZnS/C anode shows better rate performance than that of MCMB anode.

Cycling performances of ZnS/C and MCMB anode at wide-ranging temperatures were also measured to evaluate the environmental availability of the ZnS/C anode material. Fig. 7 displayed their cycling performance in various temperature range from −20 °C to 20 °C, where, the charge–discharge specific current was 400 mA/g. Before the cycling tests at various temperatures, the freshly prepared electrodes were conditioned by cycling

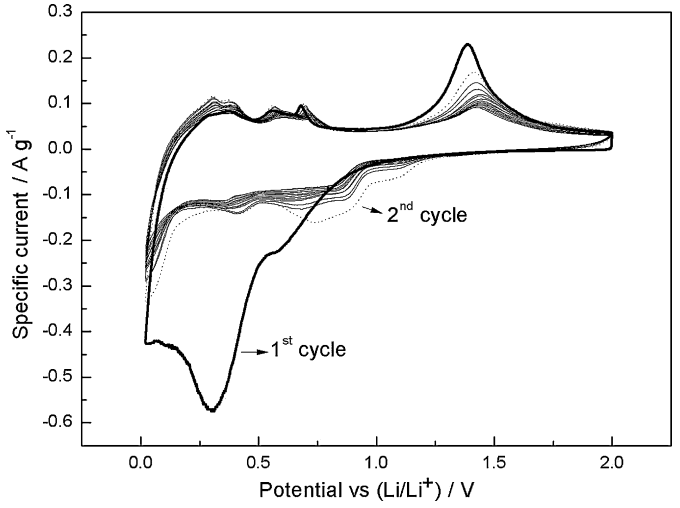

Fig. 5. Cyclic voltammograms of the ZnS/C (9.3 wt% C) electrode at a scan rate of 0.1 mV/s.

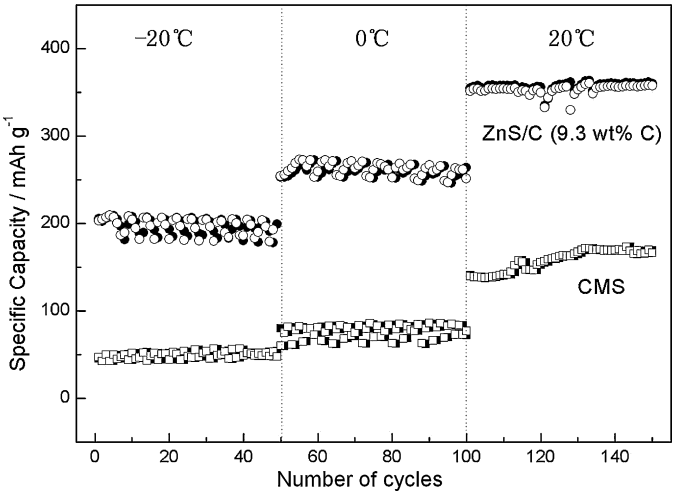

Fig. 7. Cycling performance of ZnS/C (9.3 wt% C) anode and commercial MCMB anode at wide-ranging temperature with a charge–discharge specific current of 400 mA/g.

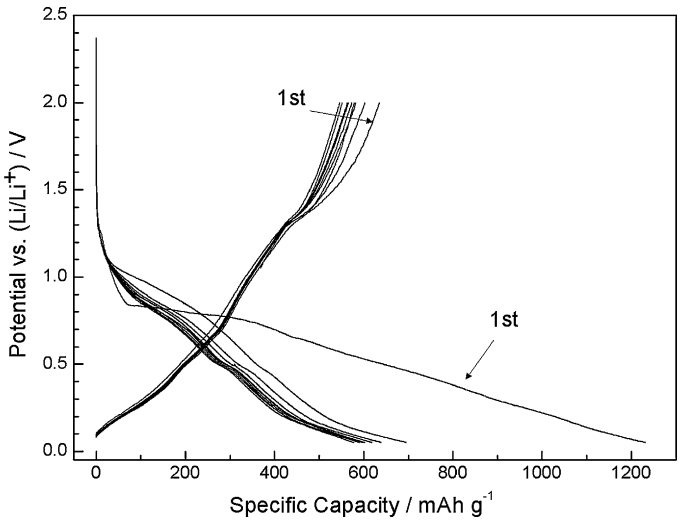

Fig. 8. Discharge and charge profiles and the cycling performance of ZnS/C at the specific current of 40 mA/g.

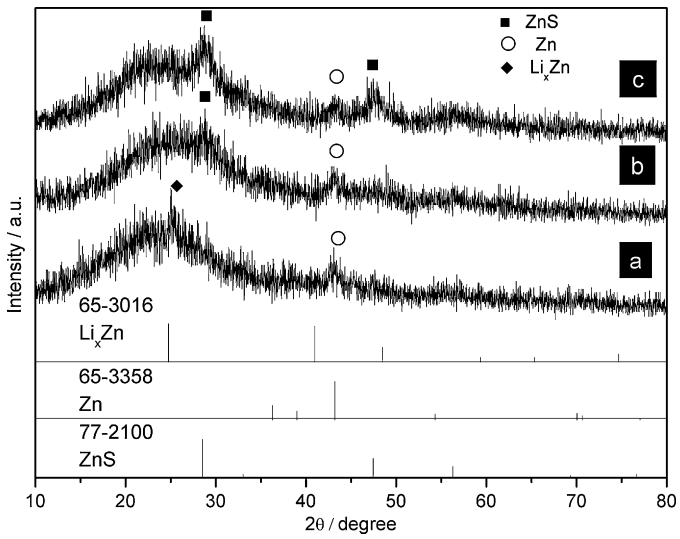

Fig. 10. Ex situ XRD patterns of ZnS/C electrode during the first cycle at different charge potentials (a: 0.05 V, b: 1.4 V, c: 2.0 V).

at 400 mA/g at room temperature for 20 cycles. As observed clearly, the MCMB anode displayed a discharge capacity less than 100 mAh/g at low temperature and is not suitable for low temperature application. However, the ZnS/C anode delivered 268 mAh/g at 0 °C and 207 mAh/g at −20 °C, which were 74.4% and 57.5% of the capacity at 20 °C. This indicated that ZnS/C composite also exhibits excellent low temperature performance even discharged at high rate.

For the investigation of the intercalation mechanism of the ZnS/C anode, the cycling performance of the ZnS/C anode has been done at a lower charge–discharge specific current. Fig. 8 presents the charge–discharge profiles of the ZnS/C anode over the potential range between 0.05 V and 2.0 V at the specific current of 40 mA/g. In the first lithium insertion process (1st cycle), a plateau forms near 0.8 V indicating the decomposition of ZnS. When lithium ions inserted into the zinc sulphide, ZnS is reduced into Zn and some of lithium–zinc alloys are generated between 0.5 V and 0.05 V. The superfluidity of zinc metal maybe benefit to the endurance of lithium insertion–extraction process of the matrix structure [20].

The phase change of the ZnS/C electrode at different discharge states is measured by ex situ XRD technique in order to clarify the lithium insertion–extraction mechanism; the first charge–discharge profile (Fig. 9) is adopted. Fig. 10 shows the XRD patterns of the ZnS/C electrodes at the potentials of 0.05 V (fully charge state), 1.4 V (about 50% discharge state) and 2.0 V (fully discharge state). It can be seen, at fully charge state (a), the peaks of ZnS disappeared and the peaks of Li_xZn and Zn are observed. The intercalation reaction of ZnS can be expressed:

$$xLi^+ + ZnS + xe^- \rightarrow Li_xS + Zn \quad (1)$$

Indicating the ZnS completely change into matrix of Li_2S, metallic Zn and the final product of Li_xZn alloy nearby the potential of 0.05 V.

From the ex situ XRD patterns corresponding to the discharged states of 1.4 V (b) and 2.0 V (c), it also can be found, the peaks of Li_xZn alloy phase disappeared and the peak of ZnS phase at 2θ of 28.57° could be detected. On further charge, the peaks of ZnS phase became clear. It is clearly that lithium is removed initially from the Li_xZn alloy to form metallic Zn firstly during the discharge process, and the lithium are extracted from Li_2S and ZnS phase formed with the discharge potential increasing. Based on the phase change of the anode active material, we deliver the lithium extraction mechanism of the ZnS/C composites as following:

$$Li_xZn\text{–}xe^- \rightarrow xLi^+ + Zn \quad (2)$$

$$Li_2S + Zn - 2e^- \rightarrow 2Li^+ + ZnS \quad (3)$$

Lithium insertion–extraction mechanism of the ZnS/C composite active electrode material can be expressed:

$$(x+2)Li^+ + ZnS + (x+2)e^- \leftrightarrow Li_2S + Li_xZn \quad (4)$$

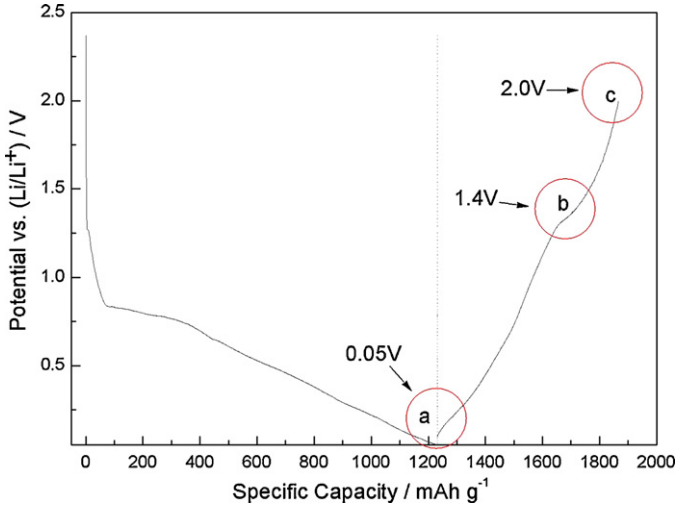

Fig. 9. First discharge and charge profile of ZnS/C electrode at the specific current of 40 mA/g.

4. Conclusions

Bare ZnS and ZnS/C composites with different carbon contents were synthesized by a precipitation method combining with carbon coating. Based on the TEM, XRD and their electrochemical behavior evaluation, bare ZnS shows lower electrochemical performance as anode active materials for lithium ion batteries. Carbon coatings are beneficial to improve the electrochemical performance of ZnS anode material. The ZnS/C electrodes present excellent microstructure with super fine ZnS nanoparticles uniformly dispersed in conductive carbon network. As a result, the ZnS/C (9.3 wt% C) anode exhibited high rate capability and appre-

ciable low temperature performance, when the carbon content increased to 11.4 wt%, the relative content of ZnS decreased and the total capacity of the composite was reduced as well. The ZnS/C (9.3 wt% C) anode demonstrated initial charge and discharge capacity of 1021.1 and 481.6 mAh/g at a large specific current of 400 mA/g, and still has a discharge capacity of 304 mAh/g after 300 cycles. An ex situ XRD study indicated that ZnS is reduced into metallic Zn and Li_xZn alloy during the first lithium insertion procedure. On the lithium extraction procedure, the peaks of Li_xZn alloy disappeared and the peaks of ZnS are detected with the increasing of the discharge potential. ZnS/C composites should become one of promising anode active material for lithium ion batteries. It can be concluded that ZnS/C composites will be a promising anode active material for rechargable lithium batteries application.

Acknowledgements

The authors are grateful for the financial support by the 973 Program of China (2007CB209705) and the Natural Science Foundation of China (20773087, 21073120). It is also to be thankful for the kindly support by the Science and Technology Commission of Shanghai Municipality (09DZ1203603, 09XD1402400 and 09HJS000100).

References

[1] J.O. Besenhard, J. Yang, M. Winter, J. Power Sources 68 (1997) 87.
[2] Y. Idota, T. Kubota, A. Matsufuji, Y. Maekawa, T. Miyasaka, Science 276 (1997) 1395.
[3] X.Z. Liao, Z.F. Ma, J.H. Hu, Y.Z. Sun, X.X. Yuan, Electrochem. Commun. 5 (2003) 657.
[4] F. Belliard, J.T.S. Irvine, J. Power Sources 97–98 (2001) 219.
[5] N. Pereira, L.C. Klein, G.G. Amatucci, J. Electrohem. Soc. 149 (2002) A262.
[6] M.V.V.M. Satya Kishore, U.V. Varadaraju, J. Power Sources 144 (2005) 204.
[7] Z.Y. Yuan, F. Huang, J.T. Sun, Y.H. Zhou, Chem. Lett. (2002) 408.
[8] A. Rong, X.P. Gao, G.R. Li, T.Y. Yan, H.Y. Zhu, J.Q. Qu, D.Y. Song, J. Phys. Chem. B 110 (2006) 14754.
[9] S. Yoon, C.M. Park, H. Kim, H.J. Sohn, J. Power Sources 167 (2005) 520.
[10] N. Jayaprakash, K. Sathiyanarayanan, N. Kalaiselvi, Electrochim. Acta 52 (2007) 2453.
[11] Y. Sharma, N. Sharma, G.V. Subba Rao, B.V.R. Chowdar, Adv. Funct. Mater. 17 (2007) 2855.
[12] T. Fujieda, S. Takahashi, S. Higuchi, J. Power Sources 40 (1992) 283.
[13] J. Wang, P. King, R.A. Huggins, Solid State Ionics 20 (1986) 185.
[14] Y. Li, J.P. Tu, X.H. Huang, H.M. Wu, Y.F. Yuan, Electrochem. Commun. 9 (2007) 49.
[15] M. Jayalakshmi, M. Mohan Rao, J. Power Sources 157 (2006) 624.
[16] J.Z. Wang, G.X. Wang, L. Yang, S.H. Ng, H.K. Liu, J. Solid State Electrochem. 10 (2006) 250.
[17] T.-J. Kim, C. Kim, D. Son, M. Choi, B. Park, J. Power Sources 167 (2007) 529.
[18] H.S. Kim, Y.H. Chung, S.H. Kang, Y.-E. Sung, Electrochim. Acta 54 (2009) 3606.
[19] F. Belliard, P.A. Connor, J.T.S. Irvine, Ionics 5 (1999) 450.
[20] C. Kim, M. Noh, M. Choi, J. Cho, B. Park, Chem. Mater. 17 (2005) 3297.